



**HAL**  
open science

## Identification of potent inhibitors of arenavirus and SARS-CoV-2 exoribonucleases by fluorescence polarization assay

Sergio Hernández, Mikael Feracci, Carolina Trajano de Jesus, Priscila El Kazzi, Rafik Kaci, Laura Garlatti, Clemence Mondielli, Fabrice Bailly, Philippe Cotelle, Franck Touret, et al.

### ► To cite this version:

Sergio Hernández, Mikael Feracci, Carolina Trajano de Jesus, Priscila El Kazzi, Rafik Kaci, et al.. Identification of potent inhibitors of arenavirus and SARS-CoV-2 exoribonucleases by fluorescence polarization assay. *Antiviral Research*, 2022, 204, pp.105364. 10.1016/j.antiviral.2022.105364 . hal-03860671

**HAL Id: hal-03860671**

**<https://hal.science/hal-03860671v1>**

Submitted on 26 Oct 2023

**HAL** is a multi-disciplinary open access archive for the deposit and dissemination of scientific research documents, whether they are published or not. The documents may come from teaching and research institutions in France or abroad, or from public or private research centers.

L'archive ouverte pluridisciplinaire **HAL**, est destinée au dépôt et à la diffusion de documents scientifiques de niveau recherche, publiés ou non, émanant des établissements d'enseignement et de recherche français ou étrangers, des laboratoires publics ou privés.

# 1 Identification of potent inhibitors of arenavirus and SARS-CoV-2 2 exoribonucleases by fluorescence polarization assay

3  
4 Sergio Hernández<sup>1</sup>, Mikael Feracci<sup>1</sup>, Carolina Trajano De Jesus<sup>1</sup>, Priscila El Kazzi<sup>1</sup>, Rafik Kaci<sup>1</sup>, Laura  
5 Garlatti<sup>1</sup>, Clemence Mondielli<sup>2</sup>, Fabrice Bailly<sup>3</sup>, Philippe Cotelle<sup>3,4</sup>, Franck Touret<sup>5</sup>, Xavier de Lamballerie<sup>5</sup>,  
6 Bruno Coutard<sup>5</sup>, Etienne Decroly<sup>1</sup>, Bruno Canard<sup>1</sup>, François Ferron<sup>1</sup> and Karine Alvarez<sup>1</sup>

7  
8 <sup>1</sup> Université Aix-Marseille, Architecture et Fonction des Macromolécules Biologiques (AFMB) – UMR7257  
9 CNRS – Case 932, 163 avenue de Luminy, Marseille CEDEX 09, 13288, France.

10 <sup>2</sup> Evotec (France) SAS, Campus Curie, 195 route d’Espagne, 31036 Toulouse CEDEX, France.

11 <sup>3</sup> Univ Lille, INSERM, CHU Lille, UMR-S 1172, Lille Neuroscience and Cognition Research Center, F-59000,  
12 Lille, France.

13 <sup>4</sup> ENSCL-Centrale Lille, CS 90108, F-59652, Villeneuve d’Ascq, France.

14 <sup>5</sup> Unité des Virus Émergents (UVE : Aix-Marseille University -IRD 190-Inserm 1207-IHU Méditerranée  
15 Infection), Marseille, France.

16  
17 Address correspondence to: Karine Alvarez and François Ferron, AFMB, Case 932, 163 avenue de Luminy,  
18 13288 Marseille Cedex 9, France, Tel:+33-491-825570, Fax:+33-491-266720, Email: karine.alvarez@univ-  
19 amu.fr and francois.ferron@univ-amu.fr.

## 20 21 Abstract

22 Viral exoribonucleases are uncommon in the world of RNA viruses. To date, they have only been identified  
23 in the *Arenaviridae* and the *Coronaviridae* families. The exoribonucleases of these viruses play a crucial role  
24 in the pathogenicity and interplay with host innate immune response. Moreover, coronaviruses  
25 exoribonuclease is also involved in a proofreading mechanism ensuring the genetic stability of the viral  
26 genome. Because of their key roles in virus life cycle, they constitute attractive target for drug design.

27 Here we developed a sensitive, robust and reliable fluorescence polarization assay to measure the  
28 exoribonuclease activity and its inhibition *in vitro*. The effectiveness of the method was validated on three  
29 different viral exoribonucleases, including SARS-CoV-2, Lymphocytic Choriomeningitis and Machupo  
30 viruses. We performed a screening of a focused library consisting of 113 metal chelators. Hit compounds were  
31 recovered with an IC<sub>50</sub> at micromolar level. We confirmed 3 hits in SARS-CoV-2 infected Vero-E6 cells.

32

33 Keywords

34 Phosphohydrolase activity, *Arenaviridae*, *Coronaviridae*, exoribonuclease activity, fluorescence polarization,  
35 screening, inhibitors, IC<sub>50</sub>, cellular assays.

36

37 Highlights

- 38 • *Arenaviridae* and *Coronaviridae* viral families share an exoribonuclease activity of common  
39 evolutionary origin
- 40 • *Arenaviridae* and *Coronaviridae* exoribonuclease is an attractive target for drug development
- 41 • We developed an activity assay using fluorescence polarization in 384 well-plates
- 42 • We validated the assay and screened a focused library of 113 metal chelators against SARS-CoV-2,  
43 Lymphocytic Choriomeningitis virus and Machupo virus exoribonucleases
- 44 • We selected several hit inhibitors and determined by fluorescence polarization their IC<sub>50</sub> at micromolar  
45 level.
- 46 • We tested hit compounds in cellular assay and we confirmed 3 hits previously detected in the *in vitro*  
47 screening out of 6 new promising SARS-Cov-2 inhibitors.

48

49 1. Introduction

50 Arenaviruses are emerging RNA viruses associated with fatal neurological and hemorrhagic diseases in hu-  
51 mans. Currently there is only ribavirin as FDA-approved antiviral. For coronaviruses, in the context of the  
52 global SARS-CoV-2 pandemic, it is essential to continue to develop potent antivirals, in support of the vaccine  
53 approach.

54 These RNA viruses encode for proteins, forming a replication/transcription complex (RTC) that orchestrates  
55 viral replication (Ferron et al., 2017; Knipe and Howley, 2013; Ogando et al., 2019). The peculiarity of  
56 *Arenaviridae* and *Coronaviridae* families, is the unique viral 3'-5'-exoribonuclease (ExoN) activity described  
57 so far (Hastie et al., 2011; Snijder et al., 2003), The ExoN activity carried by arenavirus nucleoprotein (N) or  
58 the nsp14 protein of coronavirus participates to the suppression of the host innate immune response (Martínez-  
59 Sobrido et al., 2009, 2007, 2006; Becares et al., 2016; Lei et al., 2020) , moreover the nsp14 displays an  
60 additional role in maintaining the genome integrity (Bouvet et al., 2012; Ferron et al., 2018). The arenavirus  
61 and coronavirus ExoN belonging to the same DEDD superfamily (DED/EDh subfamily), are structurally  
62 homolog (Zuo and Deutscher, 2001), and characterized by the presence of four conserved acidic residues (Asp  
63 and Glu) (Bouvet et al., 2012; Yekwa et al., 2019), essential for the binding of two metal cations ( $Mg^{2+}$  and/or  
64  $Mn^{2+}$ ) involved in the RNA hydrolysis mechanism (Steitz and Steitz, 1993), always proceeding from the 3'- to  
65 the 5'-direction.

66 Because of its biological significance to the viral life cycle, ExoN is an attractive target for drug-design  
67 (Papageorgiou et al., 2020; Subissi et al., 2014).

68 In drug development efforts using ExoN of mammarenavirus and coronavirus as targets, assays making use of  
69 radiolabeled substrate (Baddock et al., 2022; Bouvet et al., 2012; Ferron et al., 2018; Saramago et al., 2021;  
70 Yekwa et al., 2019, 2017) or mass spectrometry (Scholle et al., 2021) are available but barely adapted to HT  
71 screening. Recently, HTS assays using FRET were applied to screen SARS-CoV-2 ExoN (Canal et al., 2021;  
72 Chen et al., 2021; Rona et al., 2022).

73 Here we present a convenient method using fluorescence polarization (FP) to assess the ExoN activity and its  
74 inhibition. The recorded FP signal is altered proportionally to the size of the fluorescent RNA probe which is  
75 hydrolyzed into smaller fragments. We validate the method on SARS-CoV-2, Lymphocytic Choriomeningitis  
76 (LCMV) and Machupo viruses (MACV) ExoN. The method is sensitive, robust, amenable to miniaturization  
77 (384 well plates) and allowed us to screen a focused library of 113 metal chelators over the three-targeted viral  
78 ExoN, validating the proof-of-concept of the assay. We selected several hit inhibitors and determined by FP  
79 their  $IC_{50}$ . The hit compounds were tested in cellular assays.

80

81 2. Materials and methods

82

83 *2.1 Products and reagents.*

84 Aurintricarboxylic acid (**40**) was purchased from Acros Organics. Ribavirin (**82**) and Favipiravir (**83**) were  
85 purchased from Carbosynth. The library (113 compounds) containing phenyl-DKA, piperidiny-DKA, indolyl-  
86 DKA, benzofuranyl-DKA, triazolyl-DKA (DKA families), polyphenols (POP family), *N*-  
87 hydroxyisoquinoline-1,3-diones (HID family) and miscellaneous compounds have been described previously  
88 (Saez-Ayala et al., 2019, 2018). The hit compounds **3**, **4**, **18**, **55** and **57** have been synthesized and their  
89 synthesis will be published in due course. All compounds were resuspended in 100 % DMSO at 20 mM and  
90 stored at - 20 °C. The 22-mer RNA 5'-UGACGGCCCGGAAAACCGGGCC-3' containing FAM dye at the 5'-  
91 end (5'-FAM-RNA) was purchased from Microsynth AG (Switzerland).

92

93 *2.2 Protein expression and purification.*

94 All proteins were expressed in E. Coli. The LCMV and MACV ExoN plasmids used for this study were  
95 described in (Yekwa et al., 2019). For the expression of the SARS-CoV-2 nsp10 and nsp14, the synthetic  
96 genes were purchased from Twist Bioscience (USA). The protein production methods are detailed in the  
97 supplementary data file (see also figure S1 for elution profiles).

98

99 *2.3 Set-up of exonuclease activity conditions based on fluorescent polarization assay*

100 *2.3.1 Optimization of 5'-FAM-RNA concentration, ExoN/RNA ratio, temperature, metal ion nature and*  
101 *concentration*

102 Reactions were performed in 20 µl total volume in a buffer containing 40 mM Tris (pH 8), 5 mM DTT and 2  
103 or 5 mM MnCl<sub>2</sub>. For each 5'-FAM-RNA concentration (0.05, 0.1, 0.25, 0.5 and 1 µM), a range of concentration  
104 of ExoN was tested from a ratio of 5-fold less enzyme up to 10-fold more enzyme (0.01 to 10 µM) than 5'-  
105 FAM-RNA. For SARS-CoV-2 ExoN, the molar ratio of nsp14:nsp10 complex in the reactions was always  
106 kept at 1:4, as optimized previously (Bouvet et al., 2012) to enhance nsp14 activity.

107 To find the optimal temperature, metal ion nature and concentration, the 5'-FAM-RNA concentration was kept  
108 at 0.1 µM and ExoN concentration ranged from 0.1 to 1.6 µM. The activity was tested in the presence of MnCl<sub>2</sub>  
109 or MgCl<sub>2</sub> at 1, 2 or 5 mM. The FP signal was recorded either at 25°C or at 37°C. Negative controls tested used  
110 consisted in the replacement of MnCl<sub>2</sub> by CaCl<sub>2</sub> or, depletion of the metal ion or the enzyme. The reactions  
111 started by the addition of 5'-FAM-RNA and the fluorescence polarization (FP) was read in the Pherastar FSX

112 (BMG Labtech) using the 480 nm excitation and 520 nm emission filter, during 30 minutes at 25°C or 37°C,  
113 every 30 seconds. The gain was set up using the negative control which contained the 5'-FAM-RNA in the  
114 presence of heat-denatured nuclease. After 30 minutes, the reactions were stopped by the addition of an equal  
115 volume of loading buffer (8M urea containing 10 mM EDTA) and the digestion products were then loaded in  
116 7 M urea containing 20% (wt/vol) polyacrylamide gels (acrylamide/bisacrylamide ratio 19:1) buffered with  
117 TBE and visualized using a Fluorescent Image Analyzer Typhoon (GE Healthcare).

118

### 119 *2.3.3 Time course of ExoN assay*

120 Reactions of 20 µl total volume were performed in the buffer mentioned above, with 2 or 5 mM MnCl<sub>2</sub> for  
121 SARS-CoV-2 or arenaviruses ExoN, respectively. The 5'-FAM-RNA concentration was fixed at 0.1 µM. The  
122 SARS-CoV-2 nsp14/nsp10 ExoN complex concentration was ranged from 0.2 to 1 µM and pre-incubation at  
123 room temperature for 5 minutes was performed to allow the complex formation. The LCMV and MACV ExoN  
124 concentration was ranged from 0.1 to 1.6 µM. The reaction started with the addition of 5'-FAM-RNA and The  
125 FP signal was recorded as mentioned previously. At end point, an aliquot of the sample was examined in urea  
126 PAGE as mentioned above. The assays were done in triplicate.

127

### 128 *2.4 Screenings and IC<sub>50</sub> determination.*

129

#### 130 *2.4.1 Screenings*

131 The screenings at 5 µM and 20 µM inhibitor concentration were performed in 384-wells with flat bottom Nunc  
132 plates, in 20 µL total volume reaction. Reactions were performed in a buffer containing 40 mM Tris (pH 8), 5  
133 mM DTT, with 2 or 5 mM MnCl<sub>2</sub> for SARS-CoV-2 or arenaviruses ExoN, respectively. The 5'-FAM-RNA  
134 and ExoN concentrations were fixed at 0.1 µM. and 0.4 µM, respectively. Compounds (**1-113**) were added to  
135 the reaction with a final concentration of 5 µM and 20 µM in 5% DMSO. 8 reactions mix with ExoN were  
136 used as positive controls and 8 reactions mix with heat-denatured ExoN were used as negative controls.  
137 Reactions were initiated by adding the 5'-FAM-RNA and the FP signal was recorded as mentioned previously.  
138 To calculate the percentage of inhibition, a time correction was applied for the delayed initiation of the reaction  
139 due to the use of a multichannel pipette. The percentage of inhibition at a given time was calculated as follows:

140 
$$\text{inhibition\%} = \frac{100 \times (FP - \text{average of positive controls})}{(\text{average negative controls} - \text{average positive controls})}$$

141 where FP correspond to the fluorescent polarization signal of a compound.

142 The time selected for doing this calculation was the time when the signal of the positive control reached the  
143 plateau (30 minutes). To assess the robustness of the assay we calculate the z' value.(Formula and  
144 representative scatter plot in supplementary figure S3).

145

#### 146 *2.4.2 IC<sub>50</sub> determination*

147 Reactions were performed in the same experimental conditions as used for the screenings. The compound  
148 concentrations varied from 0.2 to 12.5 μM for LCMV ExoN, from 0.4 to 25 μM for MACV ExoN and from  
149 0.5 to 16 μM for SARS-CoV-2 ExoN nsp14/nsp10 complex. The reaction started with the addition of 5'-FAM-  
150 RNA and the FP signal was recorded as mentioned previously. The percentage of inhibition was calculated as  
151 indicated in the previous section. The curves of the percentage of inhibition with respect to the inhibitor  
152 concentration in a logarithmic scale were fitted in Graphpad Prism software using a four parameters equation.  
153 The assays were done in triplicate.

154

#### 155 *2.6 Cellular assays*

156 LCMV minigenome assays (MG) were adapted from a previously described procedure (Saez-Ayala et al.,  
157 2019, 2018). SARS-CoV-2 cellular assays were performed as previously described (Touret et al., 2021, 2020).  
158 Protocols are detailed in the supplementary data file.

159

### 160 3. Results and discussion

161

162 Fluorescence polarization (FP) is a reliable and sensitive tool for monitoring enzymatic reaction, by  
163 determining the difference of polarization signals (Zhang et al., 2012). FP - based assay is a robust method  
164 commonly used in drug discovery (Lea and Simeonov, 2011; Uri and Nonga, 2020). The FP signal recorded  
165 is proportional to the molecular weight (MW) of a fluorescent molecule (Kwok, 2002; Latif et al., 2001). We  
166 decided to apply this method to viral ExoN activity, by monitoring the size of a fluorescent-labeled RNA probe

167 which is altered in the course of the nuclease, reflecting the enzymatic activity (Liu et al., 2014; Zhang et al.,  
168 2012). The assay was first optimized.

169

### 170 *3.1 Optimization of experimental conditions of ExoN activity based on FP assay*

171

172 To set-up a screening assay, we explored 5'-FAM-RNA substrate and ExoN concentration and ratio, metal ion  
173 co-factors, temperature and reaction duration. Some RNA substrate and optimal conditions were already  
174 described (Bouvet et al., 2012; Saramago et al., 2021; Yekwa et al., 2019, 2017). A 22mer RNA that forms a  
175 stable hairpin in its 3' end has been reported to be a valuable substrate for both ExoN. Moreover, for SARS-  
176 CoV-2 ExoN, nsp10 able to stimulate nsp14 ExoN activity (Bouvet et al., 2012; Saramago et al., 2021) was  
177 added in the reaction (ratio 1:4 of nsp14:nsp10).

178 We first determined the optimal 5'-FAM-RNA concentration that provides sufficient and stable FP signal, and  
179 the ratio of ExoN and 5'-FAM-RNA. For each 5'-FAM-RNA concentration (0.05 to 1 $\mu$ M), single turnover  
180 (STO) conditions (excess of enzyme versus substrate) and also multiple turnover (MTO) conditions (excess of  
181 substrate versus enzyme) were tested. A significant change in the FP signal was observed only under STO  
182 conditions. 0.1 $\mu$ M concentration of 5'-FAM-RNA was selected to provide a reproducible and stable FP signal.  
183 To optimize the controls, several combinations were tested (Supplementary figure S2). For all negative  
184 controls, there was no variation between the initial and final FP values. However, we observe that the initial  
185 FP values are lower without MnCl<sub>2</sub>. This result is consistent with the study of Liu *et al* (Liu et al., 2014), who  
186 reported that cations can affect the FP signal. The negative controls were then prepared by mixing 5'-FAM-  
187 RNA with MnCl<sub>2</sub> and without ExoN.

188 Regarding the nature of the metal ion, MnCl<sub>2</sub> and MgCl<sub>2</sub> were tested. An increased activity is observed with  
189 MnCl<sub>2</sub> (data not shown). The concentration of MnCl<sub>2</sub> that shows the highest reduction in FP signal is 5 mM  
190 for arenaviruses (Yekwa et al., 2019, 2017) and 2 mM for SARS-CoV-2 (Baddock et al., 2020; Saramago et  
191 al., 2021). Finally, the temperature of the assay is 25°C since the incubation at 37°C leads to a significant  
192 evaporation of the sample.

193

### 194 *3.2 Assessing the SARS-CoV-2, LCMV and MACV ExoN activity by FP*

195



196 While the 5'-FAM-RNA substrate was fixed at 0.1  $\mu$ M, 0.1 to 1.6  $\mu$ M of ExoN were tested. The FP signal was  
197 measured for 30 min. The FP curves and end point RNA degradation products examined in urea PAGE, are  
198 gathered in figure 1.

199 The negative controls (figure 1, brown curves, in panels A, B and C) present flattened curves, as expected.  
200 Strikingly, a small increase in the initial FP value is observed, corresponding to the time required for the  
201 formation of the catalytic complex. This is particularly visible with SARS-CoV-2 nsp14, which requires its  
202 activation by the cofactor nsp10. Indeed, nsp14 ExoN N-terminus is flexible, when nsp10 is not bound the  
203 catalytic site of nsp14 is distorted not allowing the catalytic ions to activate the water molecule for the  
204 nucleophilic attack (Ferron et al., 2018).

205 For all tested ExoN, except for the lowest concentration, we observe a reduction of the FP signal with time.  
206 The decrease of the FP value is correlated with the hydrolysis of the 5'-FAM-RNA, as confirmed on the urea  
207 PAGE analysis (figure 1, panels D, E and F). The difference between initial and final FP value after 30 min is  
208 proportional to the number of nucleotides removed from the substrate. By increasing the ExoN concentration,  
209 we observe an increase in the FP curves slope but the FP signals reach a plateau, which might be related to the  
210 inability to remove any extra nucleotide when the RNA fragments are too shorter.

211 The method efficiency was validated by the difference of FP values between the negative control (figure 1,  
212 brown curves, in panels A, B and C) and one concentration after 30 min reaction. This difference was selected  
213 as significant enough, with  $\Delta$ FP +/- 30 to 60 units of mP. A molar ratio of 1:4 between the 5'-FAM-RNA (0.1  
214  $\mu$ M) and ExoN (0.4  $\mu$ M) was used for the screening. The robustness of the assay was assessed by calculating  
215 the z' factor (supplementary methods and figure S3). For LCMV, MACV and SARS-CoV-2 we obtained z'  
216 value of 0.72, 0.74 and 0.69, respectively.

217

### 218 *3.3 Screening of a focused library against the SARS-CoV-2, LCMV, and MACV ExoN using FP*

219 Because ExoN activity is metal-dependent, we screened a focused library of 113 metal chelators that we have  
220 previously developed (Saez-Ayala et al., 2019, 2018), in order to demonstrate the robustness of our FP method.  
221 All compounds of the library were selected on the basis of competitive inhibition by metal chelation approach.  
222 Several patterns were chosen on the chelating scaffolds, in order to explore electronic, structural, and steric  
223 features critical for the binding process and active site accommodation. Two screenings were performed using  
224 20  $\mu$ M and 5  $\mu$ M of compounds and the percentages of inhibition, deduced from FP curves, are gathered in

225 figure 2 (panels A, B, and C) and in supplementary figure S3, respectively.  
226 Aurintricarboxylic Acid (ATA, **40**), a polyphenol (POP), was included as a positive control as it has been  
227 previously described as a nuclease inhibitor (Baddock et al., 2022; Canal et al., 2021; Huang et al., 2016),  
228 acting as non-specific metal chelator (Liu et al., 2014). Compound **40** inhibits 100% of the different ExoN  
229 activity at 20  $\mu$ M (Figure 2, Table 1) and 52%, 39% and 23% at 5  $\mu$ M (Supplementary figure S3), respectively  
230 against LCMV, MACV and SARS-CoV-2 ExoN.

231 We identified 5 inhibitors (**65**, **67**, **77**, **78** and **91**) of LCMV ExoN including 3 common with MACV ExoN  
232 (Figure 2 and Table 1) with efficiency between 70 and 100% inhibition at 20  $\mu$ M. Compounds **65**, **67**, **77**, **78**  
233 belong to *N*-hydroxyisoquinoline-1,3-diones (HID) family and compound **91** belongs to  $\beta$ -diketo acid (DKA)  
234 family were previously described by us as potent specific metal chelators (Saez-Ayala et al., 2019, 2018). 9  
235 hit compounds (**18**, **40**, **46**, **55**, **68**, **77**, **78**, **91** and **92**) inhibiting SARS-CoV-2 ExoN with efficiency between  
236 70 and 100% inhibition at 20  $\mu$ M were also identified (Figure 2, Table1, Supplementary figure S3).  
237 Compounds **18** and **55** have never been described before. DKA **91** is the more efficient compound against all  
238 ExoN, showing inhibition at both 5  $\mu$ M and 20  $\mu$ M, with 87 to 100% inhibition at 20  $\mu$ M and 37 to 100%  
239 inhibition at 5  $\mu$ M.

240

#### 241 3.4 *IC<sub>50</sub> measurement of hit compounds by FP*

242 *IC<sub>50</sub>* determination was performed for all hit compounds displaying more than 70% inhibition at 20  $\mu$ M  
243 concentration. The dose-response curves and *IC<sub>50</sub>* values determined by hill plot curve fitting all hit compounds  
244 and reference compound **40**, are gathered in figure 3 and table 1. The FP curves and the end point digestion  
245 products examined in urea PAGE are gathered in Supplementary Figures S5 to S8. *IC<sub>50</sub>* determination was also  
246 performed for compounds **3**, **4**, **44** and **57** (table 1), although they did not display high inhibition during the  
247 primary screening.

248 As expected, the reference compound ATA **40** was a potent inhibitor with *IC<sub>50</sub>* values of  $7.05 \pm 0.78$ ,  $5.57 \pm$   
249  $0.41$  and  $5.50 \pm 0.19$   $\mu$ M, for LCMV, MACV and SARS-CoV-2 ExoN, respectively. The highest inhibition  
250 observed with the DKA **91** during the two screenings was confirmed in the *IC<sub>50</sub>* values. DKA **91** displayed  
251 equivalent efficiency to inhibit LCMV and MACV ExoN with respectively  $5.63 \pm 0.35$  and  $5.42 \pm 0.46$   $\mu$ M  
252 *IC<sub>50</sub>* values. The inhibition is slightly more pronounced for SARS-CoV-2 ExoN with *IC<sub>50</sub>* of  $1.86 \pm 0.16$   $\mu$ M.

253 For other hit compounds, IC<sub>50</sub> values ranged between 6 and 24 μM. Notably, these values correlated perfectly  
254 with the inhibition % obtained by both screenings at 20 and 5 μM, confirming the robustness and  
255 reproducibility of the assay. Moreover, The FP signal correlated with the degree of digestion observed upon  
256 PAGE analysis (Supplementary Figures S5 to S8). While the HID family (compounds **65**, **67**, **68**, **77** and **78**)  
257 showed a rather broad spectrum of efficacy for both arenavirus and coronavirus ExoNs, the DKA family  
258 (phenyl-DKA, piperidinyl-DKA and triazolyl-DKA, compounds **3**, **4**, **18**, **44**, **55**, **57**, **91** and **92**) showed a clear  
259 specificity for the SARS-CoV-2 ExoN.

260

### 261 *3.5 LCMV minigenome activity*

262 Arenavirus replication can be modeled using a recombinant plasmid minigenome system comprising the viral  
263 RdRp (L), the nucleoprotein (N), and a LCMV genomic RNA (Ortiz-Riaño et al., 2013). Previous studies have  
264 shown the efficiency of this method (Saez-Ayala et al., 2019). We tested the hit compounds **40**, **65**, **67**, **77**, **78**  
265 and **91**, at 100 and 50 μM. Because ribavirin (**82**) is the only licensed antiviral agent with activity against  
266 arenaviruses (McCormick et al., 1986; Moreno et al., 2011), it was chosen as a reference compound.  
267 Favipiravir (**83**), having demonstrated broad-spectrum activity against a number of RNA viruses, was also  
268 added in the screening. Since the compounds were supposed to target the polymerase function, the assay was  
269 particularly suited by measuring the GLuc reporter gene (Gluc activity %, Supplementary Figure S9). We also  
270 tested the cytotoxic effect of the compounds at 50 and 100 μM (Cell viability %, Supplementary Figure S9).  
271 The ribavirin (**82**) resulted in a 76% and 47% inhibition of GLuc activity, at 100 and 50 μM respectively, but  
272 was associated with important cytotoxic effect with 35 and 50 % cell viability, as described previously  
273 (Mendenhall et al., 2011). Unexpectedly, favipiravir (**83**) displayed weak inhibition (30% at 100 μM) without  
274 cell viability reduction (Mendenhall et al., 2011). ATA (**40**) displayed no antiviral effect, but, cytotoxicity as  
275 described previously (Andrew et al., 1999; Haimsohn et al., 2002). Compounds **65**, **67** and **77** displayed slight  
276 effect (25 to 50% inhibition) on GLuc expression but associated with cytotoxic effect, as observed for ribavirin  
277 (**82**). Compound **78** displayed weak GLuc expression inhibition (30 % at 50 μM) without cytotoxicity,  
278 compared to ribavirin (**82**).

279

### 280 *3.6 SARS-Cov-2 in vitro evaluation*

281 The full library of 113 metal chelators was screened in a SARS-CoV-2 infected cell-based assay. We  
282 performed a primary screen for SARS-Cov-2 in VeroE6 cells (Touret et al., 2020) and we used remdesivir as  
283 a reference compound (Pruijssers et al., 2020; Wang et al., 2020). This fast and reliable assay, based on the  
284 cell viability, measures the ability of a compound to prevent the cytopathic effect induced by the viral  
285 replication at 50  $\mu$ M concentration.

286 Our primary screen identified 31 hit compounds that prevent cytopathic effect by at least 40 % (Supplemental  
287 figure S10). To go further, we next performed dose-response analysis in VeroE6 TMPRSS2 (Touret et al.,  
288 2021; Weiss et al., 2021). We used VeroE6/TMPRSS2 cells to avoid off target false-positive compounds as it  
289 has been shown for Chloroquine (Hoffmann et al., 2020). Remdesivir, as reference compound, displayed EC<sub>50</sub>  
290 of 1.5 $\pm$ 1.1  $\mu$ M with CC<sub>50</sub> > 10  $\mu$ M.

291 Of the 31 primary hits, 19 compounds displaying between 40 and 100% inhibition were analyzed in dose-  
292 response assays. 7 compounds from the same family and 5 compounds displaying between 40 and 70%  
293 inhibition were set aside. Additionally, the 8 hit compounds from the biochemical screening displaying  
294 between 0 and 40% inhibition were also analyzed. Here, we confirmed the antiviral activity of ATA (**40**)  
295 against SARS-Cov-2 in cell culture (Canal et al., 2021) with EC<sub>50</sub> of 27.23 $\pm$ 20.68  $\mu$ M. We were unable to  
296 confirm primary efficiency of 6 potential hit compounds and we identified 5 compounds that displayed  
297 significant cytotoxicity.

298 Finally, we identified 4 new compounds **3**, **4**, **44**, and **57**, that displayed a robust antiviral activity with EC<sub>50</sub>  
299 between 8 and 38  $\mu$ M without cytotoxicity and 2 compounds **46** and **55** that exert a potent antiviral activity in  
300 the same range but also showing signs of cytotoxicity, without reaching the CC<sub>50</sub> value (table 1 and  
301 supplementary figure S11) . Compounds **46** and **55** were identified during the biochemical screening on the  
302 SARS-CoV-2 ExoN, confirming the ExoN targeting.

303

#### 304 4. Conclusion

305 We proved in this study that fluorescence polarization (FP) method is reliable, sensitive to monitor nuclease  
306 activity and feasible in 384-well plates. The method is robust, rapid and non-destructive allowing the  
307 visualization of the RNA substrate degradation using gels as orthogonal method of confirmation. We identified  
308 several hit inhibitors of viral arenavirus (LCMV and MACV) and coronavirus (SARS-CoV-2) ExoN activity  
309 and determined by fluorescence polarization their IC<sub>50</sub> at a micromolar level. Then we validated their activities

310 in cell culture assays and we found compounds displaying efficiency at micromolar level against SARS-CoV-  
311 2. These results highlight the effectiveness of fluorescence polarization assay in the screening of compounds  
312 libraries for the discovery of antivirals.

313

314

315

316

## 317 Funding and Acknowledgments

318 This work was supported by grants from the Ministry of the Armed Forces (DGA) – Defense Innovation  
319 Agency (AID) and the French National Research Agency (ANR-18-ASTR-0010-01, PaNuVi), Fondation pour  
320 la Recherche Medicale (Chemistry for Medecine, DCM20181039531), SCORE project H2020 SC1-PHE  
321 Coronavirus-2020 (grant#101003627). Priscila El-Kazzi and Rafik Kaci were funded by Fondation  
322 Mediterranée Infection (Infectiopole Sud), Laura Garlatti was funded by DGA and Aix-Marseille University  
323 (fellowship N° DGA01D19024292 AID). The Carolina Trajano De Jesus master's internship was supported  
324 by the Coordenação de Aperfeiçoamento de Pessoal de Nível Superior - Brasil (CAPES) – Finance Code 001.  
325 We thank Pr C Drosten for providing the SARS-CoV-2 BavPat strain through EVA GLOBAL. A part of the  
326 work was done on the Aix Marseille University antivirals drug design platform “AD2P”. We thank Thi Hong  
327 Van Nguyen and Adrien Delpal for technical assistance.

328

329 Supplementary data associated with this article can be found, in the online version, at

330

## 331 References

- 332 Andrew, D.J., Hay, A.W., Evans, S.W., 1999. Aurintricarboxylic acid inhibits apoptosis and supports  
333 proliferation in a haemopoietic growth-factor dependent myeloid cell line. *Immunopharmacology* 41,  
334 1–10. [https://doi.org/10.1016/s0162-3109\(98\)00049-6](https://doi.org/10.1016/s0162-3109(98)00049-6)
- 335 Baddock, H.T., Brolih, S., Yosaatmadja, Y., Ratnaweera, M., Bielinski, M., Swift, L.P., Cruz-Migoni, A., Fan,  
336 H., Keown, J.R., Walker, A.P., Morris, G.M., Grimes, J.M., Fodor, E., Schofield, C.J., Gileadi, O.,  
337 McHugh, P.J., 2022. Characterization of the SARS-CoV-2 ExoN (nsp14ExoN-nsp10) complex:  
338 implications for its role in viral genome stability and inhibitor identification. *Nucleic Acids Res.* 50,  
339 1484–1500. <https://doi.org/10.1093/nar/gkab1303>
- 340 Baddock, H.T., Brolih, S., Yosaatmadja, Y., Ratnaweera, M., Bielinski, M., Swift, L.P., Cruz-Migoni, A.,  
341 Morris, G.M., Schofield, C.J., Gileadi, O., McHugh, P.J., 2020. Characterisation of the SARS-CoV-2  
342 ExoN (nsp14ExoN-nsp10) complex: implications for its role in viral genome stability and inhibitor  
343 identification. *bioRxiv* 2020.08.13.248211. <https://doi.org/10.1101/2020.08.13.248211>

- 344 Becares, M., Pascual-Iglesias, A., Nogales, A., Sola, I., Enjuanes, L., Zuñiga, S., 2016. Mutagenesis of  
345 Coronavirus nsp14 Reveals Its Potential Role in Modulation of the Innate Immune Response. *J. Virol.*  
346 90, 5399–5414. <https://doi.org/10.1128/JVI.03259-15>
- 347 Bouvet, M., Imbert, I., Subissi, L., Gluais, L., Canard, B., Decroly, E., 2012. RNA 3'-end mismatch excision  
348 by the severe acute respiratory syndrome coronavirus nonstructural protein nsp10/nsp14  
349 exoribonuclease complex. *Proc. Natl. Acad. Sci.* 109, 9372–9377.  
350 <https://doi.org/10.1073/pnas.1201130109>
- 351 Canal, B., McClure, A.W., Curran, J.F., Wu, M., Ulferts, R., Weissmann, F., Zeng, J., Bertolin, A.P., Milligan,  
352 J.C., Basu, S., Drury, L.S., Deegan, T.D., Fujisawa, R., Roberts, E.L., Basier, C., Labib, K., Beale, R.,  
353 Howell, M., Diffley, J.F.X., 2021. Identifying SARS-CoV-2 antiviral compounds by screening for  
354 small molecule inhibitors of nsp14/nsp10 exoribonuclease. *Biochem. J.* 478, 2445–2464.  
355 <https://doi.org/10.1042/BCJ20210198>
- 356 Chen, T., Fei, C.-Y., Chen, Y.-P., Sargsyan, K., Chang, C.-P., Yuan, H.S., Lim, C., 2021. Synergistic Inhibition  
357 of SARS-CoV-2 Replication Using Disulfiram/Ebselen and Remdesivir. *ACS Pharmacol. Transl. Sci.*  
358 4, 898–907. <https://doi.org/10.1021/acspsci.1c00022>
- 359 Ferron, F., Subissi, L., Silveira De Moraes, A.T., Le, N.T.T., Sevajol, M., Gluais, L., Decroly, E., Vonrhein,  
360 C., Bricogne, G., Canard, B., Imbert, I., 2018. Structural and molecular basis of mismatch correction  
361 and ribavirin excision from coronavirus RNA. *Proc. Natl. Acad. Sci. U. S. A.* 115, E162–E171.  
362 <https://doi.org/10.1073/pnas.1718806115>
- 363 Ferron, F., Weber, F., de la Torre, J.C., Reguera, J., 2017. Transcription and replication mechanisms of  
364 Bunyaviridae and Arenaviridae L proteins. *Virus Res.* 234, 118–134.  
365 <https://doi.org/10.1016/j.virusres.2017.01.018>
- 366 Haimsohn, M., Beery, R., Karasik, A., Kanety, H., Geier, A., 2002. Aurintricarboxylic Acid Induces a Distinct  
367 Activation of the IGF-I Receptor Signaling within MDA-231 Cells. *Endocrinology* 143, 837–845.  
368 <https://doi.org/10.1210/endo.143.3.8681>
- 369 Hastie, K.M., Kimberlin, C.R., Zandonatti, M.A., MacRae, I.J., Saphire, E.O., 2011. Structure of the Lassa  
370 virus nucleoprotein reveals a dsRNA-specific 3' to 5' exonuclease activity essential for immune  
371 suppression. *Proc. Natl. Acad. Sci. U. S. A.* 108, 2396–2401.  
372 <https://doi.org/10.1073/pnas.1016404108>
- 373 Hoffmann, M., Mösbauer, K., Hofmann-Winkler, H., Kaul, A., Kleine-Weber, H., Krüger, N., Gassen, N.C.,  
374 Müller, M.A., Drosten, C., Pöhlmann, S., 2020. Chloroquine does not inhibit infection of human lung  
375 cells with SARS-CoV-2. *Nature* 585, 588–590. <https://doi.org/10.1038/s41586-020-2575-3>
- 376 Huang, K.-W., Hsu, K.-C., Chu, L.-Y., Yang, J.-M., Yuan, H.S., Hsiao, Y.-Y., 2016. Identification of  
377 Inhibitors for the DEDDh Family of Exonucleases and a Unique Inhibition Mechanism by Crystal  
378 Structure Analysis of CRN-4 Bound with 2-Morpholin-4-ylethanesulfonate (MES). *J. Med. Chem.* 59,  
379 8019–8029. <https://doi.org/10.1021/acs.jmedchem.6b00794>
- 380 Knipe, D.M., Howley, P.M. (Eds.), 2013. *Fields virology*, 6th ed. ed. Wolters Kluwer/Lippincott Williams &  
381 Wilkins Health, Philadelphia, PA.
- 382 Kwok, P.-Y., 2002. SNP genotyping with fluorescence polarization detection. *Hum. Mutat.* 19, 315–323.  
383 <https://doi.org/10.1002/humu.10058>
- 384 Latif, S., Bauer-Sardina, I., Ranade, K., Livak, K.J., Kwok, P.Y., 2001. Fluorescence polarization in  
385 homogeneous nucleic acid analysis II: 5'-nuclease assay. *Genome Res.* 11, 436–440.  
386 <https://doi.org/10.1101/gr.156601>
- 387 Lea, W.A., Simeonov, A., 2011. Fluorescence polarization assays in small molecule screening. *Expert Opin.*  
388 *Drug Discov.* 6, 17–32. <https://doi.org/10.1517/17460441.2011.537322>
- 389 Lei, X., Dong, X., Ma, R., Wang, W., Xiao, X., Tian, Z., Wang, C., Wang, Y., Li, L., Ren, L., Guo, F., Zhao,  
390 Z., Zhou, Z., Xiang, Z., Wang, J., 2020. Activation and evasion of type I interferon responses by  
391 SARS-CoV-2. *Nat. Commun.* 11, 3810. <https://doi.org/10.1038/s41467-020-17665-9>
- 392 Liu, X., Chen, Y., Fierke, C.A., 2014. A real-time fluorescence polarization activity assay to screen for  
393 inhibitors of bacterial ribonuclease P. *Nucleic Acids Res.* 42, e159. <https://doi.org/10.1093/nar/gku850>
- 394 Martínez-Sobrido, L., Emonet, S., Giannakas, P., Cubitt, B., García-Sastre, A., de la Torre, J.C., 2009.  
395 Identification of Amino Acid Residues Critical for the Anti-Interferon Activity of the Nucleoprotein  
396 of the Prototypic Arenavirus Lymphocytic Choriomeningitis Virus. *J. Virol.* 83, 11330–11340.  
397 <https://doi.org/10.1128/JVI.00763-09>
- 398 Martínez-Sobrido, L., Giannakas, P., Cubitt, B., García-Sastre, A., Torre, J.C. de la, 2007. Differential  
399 Inhibition of Type I Interferon Induction by Arenavirus Nucleoproteins. *J. Virol.* 81, 12696–12703.  
400 <https://doi.org/10.1128/JVI.00882-07>

401 Martínez-Sobrido, L., Zúñiga, E.I., Rosario, D., García-Sastre, A., de la Torre, J.C., 2006. Inhibition of the  
402 Type I Interferon Response by the Nucleoprotein of the Prototypic Arenavirus Lymphocytic  
403 Choriomeningitis Virus. *J. Virol.* 80, 9192–9199. <https://doi.org/10.1128/JVI.00555-06>

404 McCormick, J.B., King, I.J., Webb, P.A., Scribner, C.L., Craven, R.B., Johnson, K.M., Elliott, L.H., Belmont-  
405 Williams, R., 1986. Lassa fever. Effective therapy with ribavirin. *N. Engl. J. Med.* 314, 20–26.  
406 <https://doi.org/10.1056/NEJM198601023140104>

407 Mendenhall, M., Russell, A., Juelich, T., Messina, E.L., Smee, D.F., Freiberg, A.N., Holbrook, M.R., Furuta,  
408 Y., de la Torre, J.-C., Nunberg, J.H., Gowen, B.B., 2011. T-705 (Favipiravir) Inhibition of Arenavirus  
409 Replication in Cell Culture. *Antimicrob. Agents Chemother.* 55, 782–787.  
410 <https://doi.org/10.1128/AAC.01219-10>

411 Moreno, H., Gallego, I., Sevilla, N., de la Torre, J.C., Domingo, E., Martín, V., 2011. Ribavirin Can Be  
412 Mutagenic for Arenaviruses  $\nu$ . *J. Virol.* 85, 7246–7255. <https://doi.org/10.1128/JVI.00614-11>

413 Ortiz-Riaño, E., Cheng, B.Y.H., Carlos de la Torre, J., Martínez-Sobrido, L., 2013. Arenavirus reverse genetics  
414 for vaccine development. *J. Gen. Virol.* 94, 1175–1188. <https://doi.org/10.1099/vir.0.051102-0>

415 Papageorgiou, N., Spiliopoulou, M., Nguyen, T.-H.V., Vaitopoulou, A., Laban, E.Y., Alvarez, K.,  
416 Margiolaki, I., Canard, B., Ferron, F., 2020. Brothers in Arms: Structure, Assembly and Function of  
417 Arenaviridae Nucleoprotein. *Viruses* 12. <https://doi.org/10.3390/v12070772>

418 Pruijssers, A.J., George, A.S., Schäfer, A., Leist, S.R., Gralinski, L.E., Dinnon, K.H., Yount, B.L., Agostini,  
419 M.L., Stevens, L.J., Chappell, J.D., Lu, X., Hughes, T.M., Gully, K., Martinez, D.R., Brown, A.J.,  
420 Graham, R.L., Perry, J.K., Du Pont, V., Pitts, J., Ma, B., Babusis, D., Murakami, E., Feng, J.Y., Bilello,  
421 J.P., Porter, D.P., Cihlar, T., Baric, R.S., Denison, M.R., Sheahan, T.P., 2020. Remdesivir Inhibits  
422 SARS-CoV-2 in Human Lung Cells and Chimeric SARS-CoV Expressing the SARS-CoV-2 RNA  
423 Polymerase in Mice. *Cell Rep.* 32, 107940. <https://doi.org/10.1016/j.celrep.2020.107940>

424 Rona, G., Zeke, A., Miwatani-Minter, B., de Vries, M., Kaur, R., Schinlever, A., Garcia, S.F., Goldberg, H.V.,  
425 Wang, H., Hinds, T.R., Bailly, F., Zheng, N., Cotelte, P., Desmaële, D., Landau, N.R., Dittmann, M.,  
426 Pagano, M., 2022. The NSP14/NSP10 RNA repair complex as a Pan-coronavirus therapeutic target.  
427 *Cell Death Differ.* 29, 285–292. <https://doi.org/10.1038/s41418-021-00900-1>

428 Saez-Ayala, M., Laban Yekwa, E., Mondielli, C., Roux, L., Hernández, S., Bailly, F., Cotelte, P., Rogolino,  
429 D., Canard, B., Ferron, F., Alvarez, K., 2019. Metal chelators for the inhibition of the lymphocytic  
430 choriomeningitis virus endonuclease domain. *Antiviral Res.* 162, 79–89.  
431 <https://doi.org/10.1016/j.antiviral.2018.12.008>

432 Saez-Ayala, M., Yekwa, E.L., Carcelli, M., Canard, B., Alvarez, K., Ferron, F., 2018. Crystal structures of  
433 Lymphocytic choriomeningitis virus endonuclease domain complexed with diketo-acid ligands. *IUCrJ*  
434 5, 223–235. <https://doi.org/10.1107/S2052252518001021>

435 Saramago, M., Bárria, C., Costa, V., Souza, C.S., Viegas, S.C., Domingues, S., Lousa, D., Soares, C.M.,  
436 Arraiano, C.M., Matos, R.G., 2021. New targets for drug design: Importance of nsp14/nsp10 complex  
437 formation for the 3'-5' exoribonucleolytic activity on SARS-CoV-2. *bioRxiv* 2021.01.07.425745.  
438 <https://doi.org/10.1101/2021.01.07.425745>

439 Scholle, M.D., Liu, C., Deval, J., Gurard-Levin, Z.A., 2021. Label-Free Screening of SARS-CoV-2 NSP14  
440 Exonuclease Activity Using SAMDI Mass Spectrometry. *SLAS Discov. Adv. Life Sci. R D* 26, 766–  
441 774. <https://doi.org/10.1177/24725552211008854>

442 Snijder, E.J., Bredenbeek, P.J., Dobbe, J.C., Thiel, V., Ziebuhr, J., Poon, L.L.M., Guan, Y., Rozanov, M.,  
443 Spaan, W.J.M., Gorbalenya, A.E., 2003. Unique and Conserved Features of Genome and Proteome of  
444 SARS-coronavirus, an Early Split-off From the Coronavirus Group 2 Lineage. *J. Mol. Biol.* 331, 991–  
445 1004. [https://doi.org/10.1016/S0022-2836\(03\)00865-9](https://doi.org/10.1016/S0022-2836(03)00865-9)

446 Steitz, T.A., Steitz, J.A., 1993. A general two-metal-ion mechanism for catalytic RNA. *Proc. Natl. Acad. Sci.*  
447 *U. S. A.* 90, 6498–6502. <https://doi.org/10.1073/pnas.90.14.6498>

448 Subissi, L., Imbert, I., Ferron, F., Collet, A., Coutard, B., Decroly, E., Canard, B., 2014. SARS-CoV ORF1b-  
449 encoded nonstructural proteins 12-16: replicative enzymes as antiviral targets. *Antiviral Res.* 101,  
450 122–130. <https://doi.org/10.1016/j.antiviral.2013.11.006>

451 Touret, F., Driouich, J.-S., Cochin, M., Petit, P.R., Gilles, M., Barthélémy, K., Moureau, G., Mahon, F.-X.,  
452 Malvy, D., Solas, C., de Lamballerie, X., Nougairède, A., 2021. Preclinical evaluation of Imatinib  
453 does not support its use as an antiviral drug against SARS-CoV-2. *Antiviral Res.* 193, 105137.  
454 <https://doi.org/10.1016/j.antiviral.2021.105137>

455 Touret, F., Gilles, M., Barral, K., Nougairède, A., van Helden, J., Decroly, E., de Lamballerie, X., Coutard, B.,  
456 2020. In vitro screening of a FDA approved chemical library reveals potential inhibitors of SARS-  
457 CoV-2 replication. *Sci. Rep.* 10, 13093. <https://doi.org/10.1038/s41598-020-70143-6>

458 Uri, A., Nonga, O.E., 2020. What is the current value of fluorescence polarization assays in small molecule  
459 screening? *Expert Opin. Drug Discov.* 15, 131–133. <https://doi.org/10.1080/17460441.2020.1702966>  
460 Wang, M., Cao, R., Zhang, L., Yang, X., Liu, J., Xu, M., Shi, Z., Hu, Z., Zhong, W., Xiao, G., 2020. Remdesivir  
461 and chloroquine effectively inhibit the recently emerged novel coronavirus (2019-nCoV) in vitro. *Cell*  
462 *Res.* 30, 269–271. <https://doi.org/10.1038/s41422-020-0282-0>  
463 Weiss, A., Touret, F., Baronti, C., Gilles, M., Hoen, B., Nougairède, A., Lamballerie, X. de, Sommer, M.O.A.,  
464 2021. Niclosamide shows strong antiviral activity in a human airway model of SARS-CoV-2 infection  
465 and a conserved potency against the Alpha (B.1.1.7), Beta (B.1.351) and Delta variant (B.1.617.2).  
466 *PLOS ONE* 16, e0260958. <https://doi.org/10.1371/journal.pone.0260958>  
467 Yekwa, E., Aphibanthamakit, C., Carnec, X., Picard, C., Canard, B., Baize, S., Ferron, F., 2019. Arenaviridae  
468 exoribonuclease presents genomic RNA edition capacity. *bioRxiv* 541698.  
469 <https://doi.org/10.1101/541698>  
470 Yekwa, E., Khourieh, J., Canard, B., Papageorgiou, N., Ferron, F., 2017. Activity inhibition and crystal  
471 polymorphism induced by active-site metal swapping. *Acta Crystallogr. Sect. Struct. Biol.* 73, 641–  
472 649. <https://doi.org/10.1107/S205979831700866X>  
473 Zhang, M., Le, H.-N., Wang, P., Ye, B.-C., 2012. A versatile molecular beacon-like probe for multiplexed  
474 detection based on fluorescence polarization and its application for a resettable logic gate. *Chem.*  
475 *Commun. Camb. Engl.* 48, 10004–10006. <https://doi.org/10.1039/c2cc35185d>  
476 Zuo, Y., Deutscher, M.P., 2001. Exoribonuclease superfamilies: structural analysis and phylogenetic  
477 distribution. *Nucleic Acids Res.* 29, 1017–1026.  
478

479

480

481



482 Legend to figures

483

484 Figure 1. ExoN activity measured by FP for LCMV (panel A), MACV (panel B) and SARS-CoV-2 (panel C).

485 The FP signal variation is recorded with time during 30 min, each 30 secondes, at 25°C. The 5'-FAM-RNA

486 substrate concentration used is 0.1  $\mu\text{M}$  and the ExoN concentration tested ranges 0.1  $\mu\text{M}$  to 1.6  $\mu\text{M}$ . The data

487 represents the average and SEM of three independent experiments. The \* shows the enzyme concentrations at

488 which the FP values are significantly different compared to the control condition (no enzyme) \* p value < 0.05,

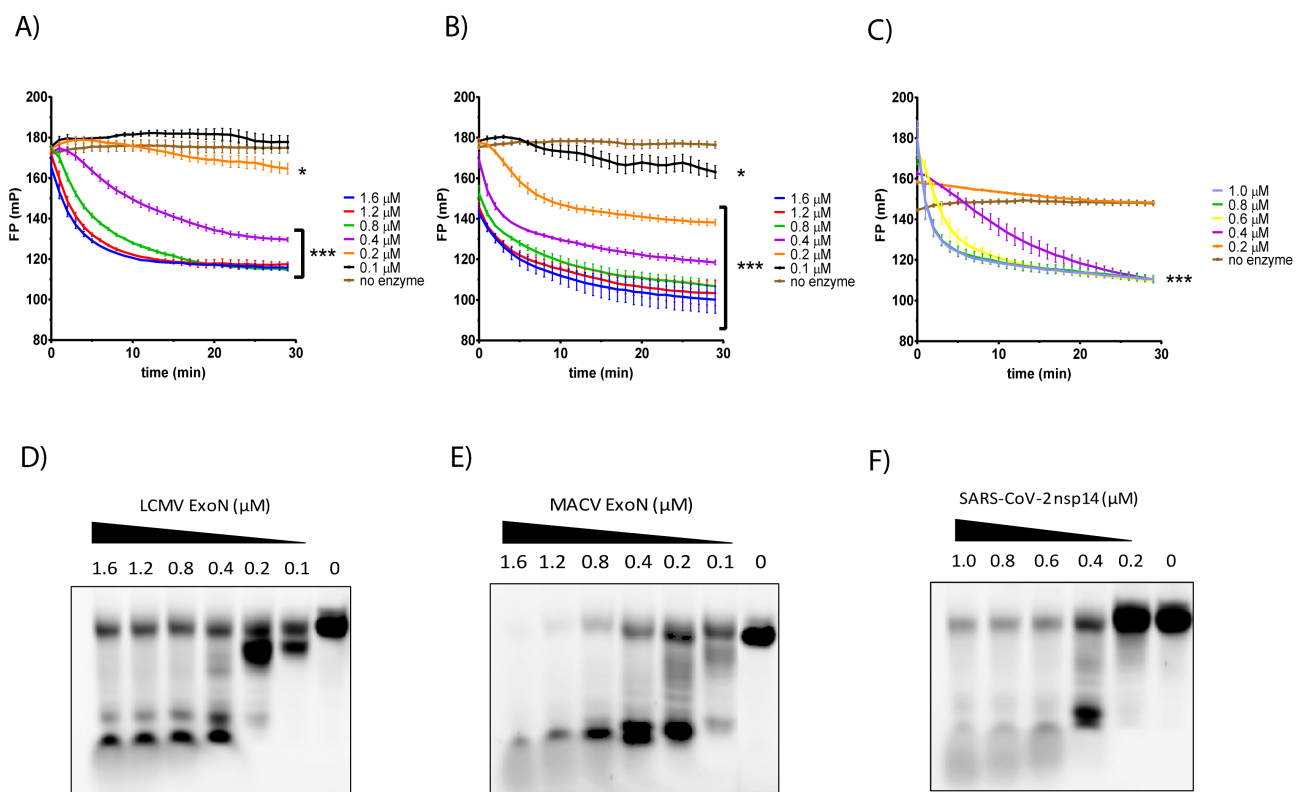
489 \*\*\* p value < 0.001 (One-way ANOVA). The bottom panels illustrate a representative image of the digestion

490 products analyzed in urea PAGE, of the ExoN activity for LCMV (panel D), MACV (panel E) and SARS-

491 CoV-2 (panel F), after recording the FP signal. An aliquot of the sample was loaded into a urea-PAGE 20%

492 and scanned in a fluorescence imager.

493



494

495

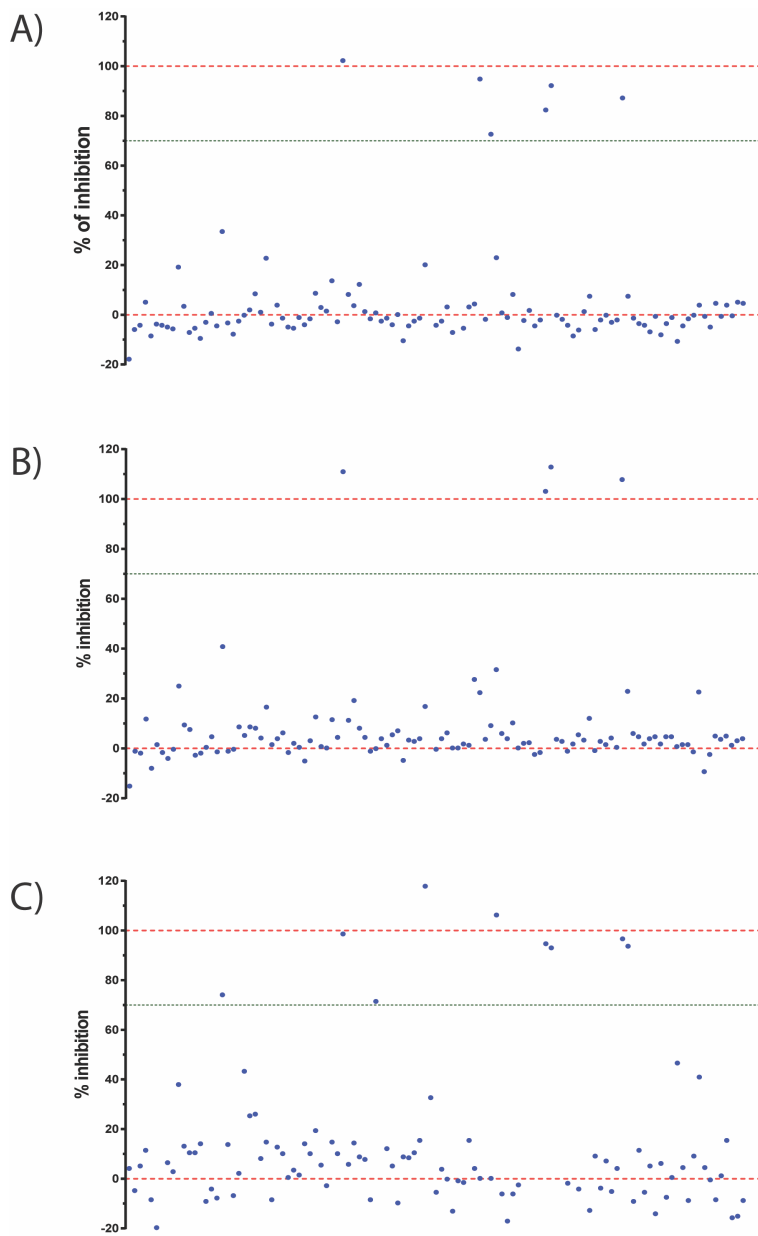
496

497

498

499 Figure 2. Screening of focused library of metal chelators (113) against LCMV (panel A), MACV (panel B)  
500 and SARS-CoV-2 nsp14:nsp10 complex (panel C) ExoN followed by FP. The dots show the % of inhibition  
501 of the ExoN activity as described in materials and methods. For the screening conditions 0.1  $\mu$ M 5'-FAM-  
502 RNA, 0.4  $\mu$ M ExoN and 20  $\mu$ M of inhibitor were used.

503



504

505

506

507

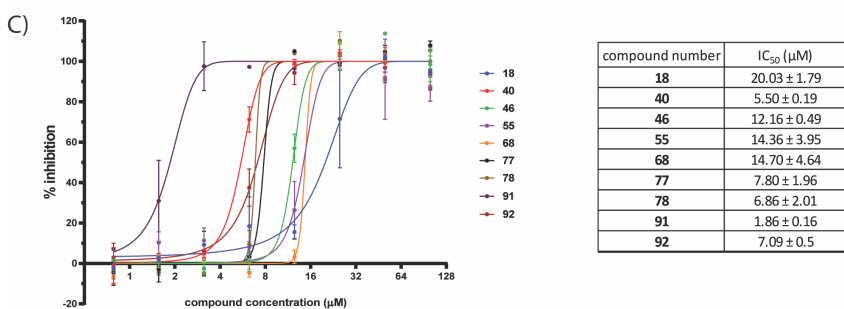
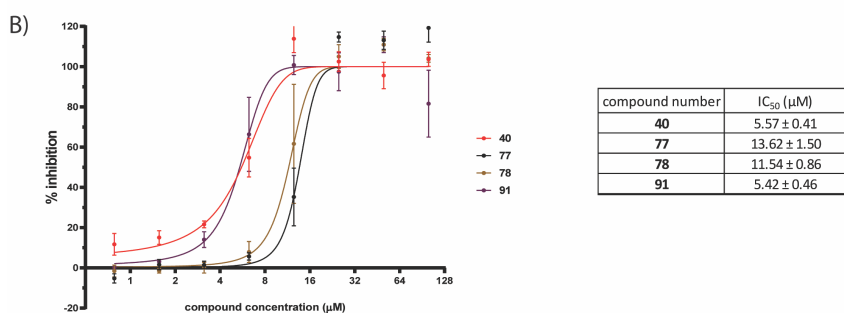
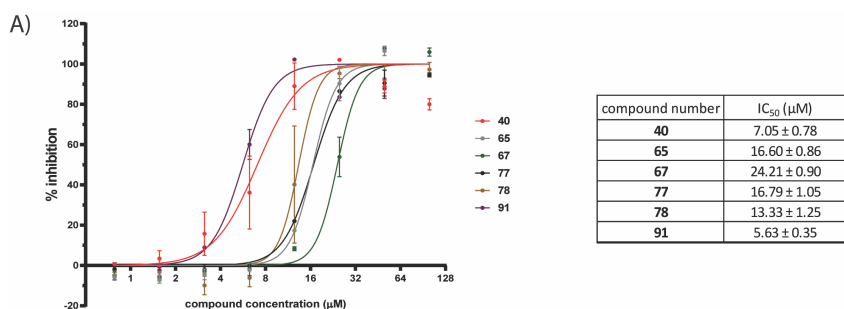
508

509

510

511 Figure 3. IC<sub>50</sub> measurement of hit compounds by FP on LCMV, MACV and SARS-CoV-2 nsp14:nsp10  
512 complex The graphs show the dose-response curves obtained by extraction of FP data and the corresponding  
513 IC<sub>50</sub> values for LCMV (panel A), MACV (panel B) and SARS-CoV-2 (panel C). The data represents the  
514 average and SEM of three independent experiments.

515

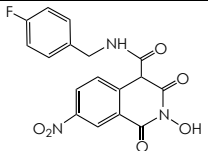
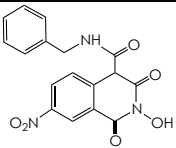
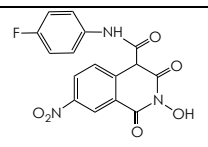
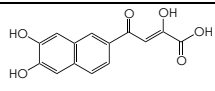
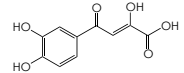


516

517 Table 1: List of hits compounds, targets, % of inhibition of the ExoN screening at 20 $\mu$ M , ExoN- IC<sub>50</sub> values,  
 518 % of inhibition of the cellular screenings at 50 $\mu$ M, EC<sub>50</sub> and CC<sub>50</sub> values and compound structures. \* :  
 519 monuplicate.

520

Cmpd N°	Target	% inhib ExoN (20 $\mu$ M)	IC <sub>50</sub> ( $\mu$ M)	% inhib Cellular Assay (50 $\mu$ M)	EC <sub>50</sub> ( $\mu$ M) CC <sub>50</sub> ( $\mu$ M)	structure
3	SARS-CoV-2	5	> 50	50	38 $\pm$ 3 > 50	
4	SARS-CoV-2	11	33.8*	70	19 $\pm$ 3.7 > 50	
18	SARS-CoV-2	74	20 $\pm$ 1.8	15	> 50 > 50	
40	LCMV MACV SARS-CoV-2	102 111 99	7.1 $\pm$ 0.8 5.6 $\pm$ 0.4 5.5 $\pm$ 0.2	0 ND 80	ND ND 27 $\pm$ 20 > 50	
44	SARS-CoV-2	8	> 50	70	26 $\pm$ 1.7 > 50	
46	SARS-CoV-2	71	12 $\pm$ 0.5	40	12 $\pm$ 3.7 > 25	
55	SARS-CoV-2	118	14 $\pm$ 4	15	23 $\pm$ 3.7 > 50	
57	SARS-CoV-2	-5	> 50	64	8.5 $\pm$ 1.3 > 50	
65	LCMV	95	16 $\pm$ 0.9	33 > 50	ND	
67	LCMV	73	24 $\pm$ 0.9	39 > 50	ND	

68	SARS-CoV-2	106	14.7 ± 4.6	10	> 50 > 50	
77	LCMV	82	16.8 ± 1.1	27	ND	
	MACV	103	13.6 ± 1.5	> 50 ND	ND	
	SARS-CoV-2	95	7.8 ± 2	0	> 50 > 50	
78	LCMV	92	13.3 ± 1.3	31	ND	
	MACV	113	11.5 ± 0.9	> 100 ND	ND	
	SARS-CoV-2	93	6.9 ± 2	0	> 50 > 50	
91	LCMV	87	5.6 ± 0.4	0	ND	
	MACV	108	5.4 ± 0.5	ND	ND	
	SARS-CoV-2	97	1.9 ± 0.2	0	> 50 > 50	
92	SARS-CoV-2	93	7.1 ± 0.5	0	> 50 > 50	

521

522

523